PAPER Nr. : 61

PERIODIC CONTROL OF THE INDIVIDUAL-BLADE-CONTROL HELICOPTER ROTOR

by

Robert M. McKillip, Jr.

M.I.T.

Cambridge, Massachusetts, U.S.A.

TENTH EUROPEAN ROTORCRAFT FORUM

AUGUST 28 – 31, 1984 – THE HAGUE, THE NETHERLANDS

Periodic Control of the Individual-Blade-Control Helicopter Rotor

Robert M. McKillip, Jr.
VTOL Technology Laboratory
Department of Aeronautics and Astronautics
Massachusetts Institute of Technology
Cambridge, Massachusetts, 02139

Abstract

This paper describes the results of an investigation into methods of controller design for linear periodic systems utilizing an extension of modern control methods. Trends present in the selection of various cost functions are outlined, and closed-loop controller results are demonstrated for two cases: first, on an analog computer simulation of the rigid out-of-plane flapping dynamics of a single rotor blade, and second, on a four foot diameter single-bladed model helicopter rotor in the M.I.T. 5x7 subsonic wind tunnel, both for various high levels of advance ratio. It is shown that modal control using the IBC concept is possible over a large range of advance ratios with only a modest amount of computational power required.

Introduction

To further expand the utility and performance of the modern helicopter, improvements must be made in the response of the aircraft to the many and varied disturbances present in its normal operation. These responses are primarily of aerodynamic origin, and are transmitted to the vehicle through its rotating blades. Thus, if sufficient action is taken at the source of these problems, it would appear possible to considerably improve the helicopter's handling qualities, reduce vibration and increase overall stability. Recent efforts to apply active control technology to rotary wings have shown promise in reducing response due to atmospheric turbulence [1,2], retreating blade stall [3], vibration suppression [4,5], blade-fuselage interference [6], and flap-lag modal damping enhancement [7].

These applications have all used the method of active pitch control to produce counteracting aerodynamic forces, but the generation of the control actuation can be divided into two fundamentally different approaches. The first and currently more widely used in vibration suppression is Higher-Harmonic-Control (HHC) [4,5,8,9,10], where integral multiples of rotor rotational frequency are appropriately scaled and phase shifted so as to generate pitch commands, either open- or closed-loop, that approximately cancel the harmonics of vibration passed down from the rotor to the fuselage. The second and more versatile of the two is Individual-Blade-Control (IBC) [1,3,6,7,11,12,13,14], involving the control of the pitch of each blade individually in the rotating frame of reference. This latter approach is essentially a "broad-band" control of the rotor blade dynamics, as opposed to the HHC limitation of discrete frequency disturbance suppression, and as such is capable of aeroelastic control of the blade modal responses to both external disturbances and pilot commands.

Since the control and the motion sensing of the IBC system is done in the rotating blade's frame of reference, the equations describing the dynamics will contain coefficients that are periodic functions of blade azimuth angle due to the rotor's non-uniform flowfield in forward flight [15]. This time dependence of the system dynamics thus makes the use of standard time-invariant controller design techniques invalid for flight speeds exhibiting moderate levels of periodicity. Hence, a definite need exists for rules and guidelines in the selection of a controller design for systems with periodic coefficients if the IBC concept is to become a piece of flight hardware.

The sections in this paper fill this gap in knowledge and experience in designing modern control systems for linearly periodic systems through a methodical series of investigations culminating in the periodic control of a model helicopter rotor in forward flight. First, the equations of motion for a single helicopter rotor blade in forward flight are presented in Section 2.

Section 3 presents modern control theory in the context of periodically varying systems, with some numerical results concerning trends in closed-loop pole locations with changes in the cost function. An extension is made in the theory to handle implicit-model-following controller design for periodic systems, and an efficient computational technique for calculating the feedback and feedforward gains is outlined.

This research was sponsored by the Ames Research Center, NASA, Moffett Field, California 94035.

In Section 4, the system identification problem for linear periodic systems is treated in two parts. First, a novel technique for estimating rotor states using position and acceleration measurements is described. The method is unique in that it contains no periodically varying elements in its observer structure. Second, a least-squares procedure for extracting the periodic system coefficients is explained. The regression uses the state estimates of the observer in its computations.

Section 5 is devoted to describing the hardware used in the various experiments conducted in the thesis. The analog computer board that simulates the out-of-plane rotor flapping dynamics is diagrammed, and then the actual model helicopter rotor system is described.

Section 6 contains experimental results. These encompass work done on the analog simulation concerning state estimation, parameter identification and closed-loop control, as well as data from the actual rotor at high advance ratios. Parameter identification trials and closed-loop controller results are detailed for the wind tunnel test data, and comparisons both with theory and with the results from the simulation tests are made.

Conclusions from this research are drawn in Section 7, and recommendations for areas of further work are given.

2. Flapping Equation of Motion

From [16] the flapping equation of motion is:

$$\frac{\ddot{\beta}}{\Omega^2} + M_{\dot{\beta}/\Omega}\frac{\dot{\beta}}{\Omega} + M_{\beta}\,\beta = M_{\theta}\,\theta \qquad (2.1)$$

where the coefficients are:

$$M_{\dot{\beta}/\Omega} = (1):\gamma\left|\frac{1}{8} - \xi\frac{1}{24}(\xi+\xi^2+\xi^3) + \mu\sin(\psi)\left(\frac{1}{6} - \frac{1}{2}(\xi+\xi^2)\right)\right|$$

$$(2):\ [(1)] + \gamma\left(\frac{1}{1-\xi}\right)\left|\frac{1}{12}(\mu\sin(\psi)-\xi)(\mu\sin(\psi)+\xi)^3\right|$$

$$(3):\ -[(1)]$$

$$M_{\beta} = (1):\ \nu^2 + \gamma\,\mu\cos(\psi)\left|\frac{1}{6}\left(1+\frac{1}{2}\xi\right)(1-\xi) + \mu\sin(\psi)\frac{1}{4}(1-2\xi)(1+\xi)\right|$$

$$(2):\ [(1)] - \gamma\left(\frac{1}{1-\xi}\right)\mu\cos(\psi)\left|\frac{1}{6}(\mu\sin(\psi)+\xi)^3\right|$$

$$(3):\ -[(1)]$$

$$M_{\theta} = (1):\ \gamma\left|\frac{1}{8} - \frac{1}{24}(\xi+\xi^2+\xi^3) + \mu\sin(\psi)\left[\frac{1}{3} - \frac{1}{6}(\xi+\xi^2)\right] + (\mu\sin(\psi))^2\left(\frac{1}{4} - \frac{1}{4}\xi\right)\right|$$

$$(2):\ [(1)] - \gamma\left(\frac{1}{1-\xi}\right)\frac{1}{12}(\mu\sin(\psi)+\xi)^4$$

$$(3):\ -[(1)]$$

The three regimes indicated correspond to: (1) normal flow, encountered over azimuth angles such that ($-\xi < \mu \sin(\psi) < \mu$); (2) mixed flow, where part of the span is in normal flow and part is in reversed flow, encountered over the the range of azimuth angles such that ($-1 < \mu \sin(\psi) < -\xi$); and (3) reversed flow, where the full blade span is in reversed flow, valid where ($\mu \sin(\psi) < -1$). This third category can obviously only exist for rotors operating at advance ratios greater than unity.

Plots of these three moment coefficients can be seen in figure 1, 2 and 3 as a function of advance ratio. A few important aspects can be seen in these time histories. Most apparent is the increase of higher harmonic content in each of the coefficients with increasing advance ratio. This is due to the fact that all the periodic terms in the coefficients enter the expression as products of advance ratio and sines or cosines of azimuth angle. As advance ratio increases, these terms dominate the coefficient's character. Second, the flap damping term never changes sign, although its value does become quite small for certain regions near the boundary between regions (2) and (3) on the retreating side. This makes sense since the local velocity due to any flapping motion would produce section angle of attack changes, generating in-phase lift forces that would oppose the motion (for the quasi-static case). And finally, the control moment due to changes in pitch angle can be seen to pass through zero on the retreating side for high advance ratios. This is due to the lift in the normal regime on the outboard span of the blade exactly cancelling the lift in the reversed flow region on the inboard section. These first two observations will help the evaluation of the parameter identification results that follow in a later chapter, and the last effect will be seen to produce singularities for certain types of controller designs.

3. Model-Following Systems

3.1 Introduction

As any helicopter engineer knows, a successful rotor system must be designed and built with careful attention given to its aeroelastic properties. Control over the many natural frequencies present in the rigid and elastic modes must be maintained in order to limit vibration, reduce blade stresses and prolong blade life. This includes the avoidance of resonances at integer multiples of rotor rotation frequency to prevent large modal excitations due to the aerodynamic forcing of the harmonic rotor wake. As was demonstrated in [16], standard linear-quadratic regulator (LQR) approaches to penalize excursions in flapping response result in closed-loop systems with a high bandwidth. This is not particularly desirable, because: (1) there may be interaction effects with other modes not accounted for in the math model that are destabilizing at such high bandwidth (gain) values; (2) the closed-loop natural frequencies may fall close to an integer multiple of rotation frequency and thus promote possible aerodynamic forcing; and (3) the large gain values may be difficult to implement in the controller hardware.

Problems exist even for the other cost functions considered that included some penalty on state rate deviations. While these provide a means of reducing controller bandwidth, they do not offer much promise in specifying the level of periodicity in the closed-loop system. Thus, tight control over a mode would require an excessive amount of iteration in order to generate the desired eigenvector structure.

Because of these drawbacks, a straightforward LQR approach to rotor blade modal control could run into serious difficulty. However, many other cost functions are possible for controller design using modern methods, the most useful for this case probably being model-following. Model-following entails expressing in the cost function a desire for the plant being controlled to possess dynamics similar to some prototype system. This prototype can be either be a physical (often electronic) system, such as for explicit model-following [17], or an implied dynamic structure, as realized through selection of the elements in the weighting matrices [18,19]. The appeal of this technique for periodic system control is twofold. First, the desired pole locations of the closed-loop system can be achieved by incorporating them into the model, and then forcing the system to emulate the model through liberal weighting of the difference between the two in the cost function. Second, control over the level of periodicity can be achieved through the same technique -- proposing a model with as much (or as little) periodicity desired and penalizing the deviations from it.

This latter feature is especially attractive for helicopter rotor control. Since the lift, propulsion and control of the helicopter are all accomplished through the rotor system, increased control over the blade response to pilot commands, flight condition and atmospheric disturbances would provide a better handling vehicle. Pilot stick deflections are essentially magnitude and direction commands on the rotor thrust vector -- any deviation of this resultant force from the desired constitutes degraded performance. Such a deviation might come from a sub- and super-harmonic response of the periodic blade dynamics, translating into a wobbling of the tip-path-plane of the rotor and possible instability at high forward speed. For this reason, then, the periodic nature of the flapping dynamics is considered a nuisance, something to be reduced through feedback control.

The model used as the prototype for this design study (and subsequent test) was that of the hover flapping dynamics, although this choice is somewhat arbitrary. This particular choice of model has the advantage that: (1) the feedback gains go to zero at hover; (2) the model is a constant-coefficient system, helping to reduce the periodicity of the closed-loop system in forward flight (and augment its stability); (3) the bandwidth of the model is well defined and thus should produce a controller without modal interaction problems; and (4) a stability-augmentation system for a full-scale helicopter would be greatly simplified if the rotor dynamics, due to inner-loop control, were relatively constant throughout the flight envelope.

3.2 Implicit-Model-Following with Input Feedforward

As mentioned above, model-following for linear-quadratic regulator design can take two forms, either explicit or implicit. In explicit-model-following, an external analog system is used as a prefilter, or command generator, to provide reference signals for the system being controlled. The cost function is a simple weighted quadratic in the difference between the outputs of this analog system and the actual plant. The resulting controller has not only feedback gains on the state variables of the plant, but also feedforward gains on the states of the analog model. This is an unfortunate (but not very surprising) result, since it requires the construction of additional hardware for the analog model, as well a means of implementing the feedforward gains.

Implicit-model-following, however, is not so demanding on closed-loop system complexity. By formulating the cost function to penalize the difference between the time derivative of the state vector and the desired model accelerations, a set of weighting matrices is arrived at that are functions only of the plant state and control vectors. This results in a set of gains that are only as numerous as the number of states. For a constant-coefficient plant, this saving in hardware may not be significant; for a periodic system it could be substantial due to the need to program time-varying gains. Because of this reduced hardware requirement, the approach taken in this paper was to use the implicit-model form.

The model-following approaches described in the previous paragraphs are regulator-type designs, in that no mention was made of including command inputs. These can be incorporated through various means, such as augmenting the state with a vector differential equation whose initial conditions can be altered to produce typical command histories, or by including the command signal explicitly in the model dynamics [19]. Due to our ever-present constraint on system order, we will develop the gain equations for the latter approach.

Given the system:

$$\dot{x}(t) = A(t)\, x(t) + B(t)\, u(t) \qquad (3.1)$$

and the model:

$$\dot{x}_m(t) = F\, x(t) + G\, d(t) \qquad (3.2)$$

where d(t) represents input commands to the model, consider a cost function penalizing deviations in accelerations according to:

$$J = (1/2) \int_0^\infty \{ (\dot{x} - \dot{x}_m)' Q (\dot{x} - \dot{x}_m) + u' R\, u \}\, dt \qquad (3.3)$$

Substitution of (3.1) and (3.2) into the above integral gives, after some algebra:

$$J = (1/2) \int_0^\infty \{ x' Wxx\, x + u' Wuu\, u + d' Wdd\, d + 2\, x' Wxu\, u - 2\, x' Wxd\, d - 2\, d' Wdu\, u \}\, dt \qquad (3.4)$$

where:

$$Wxx = (A - F)' Q (A - F)$$

$$Wuu = (R + B' Q B)$$

$$Wdd = G' Q G$$

$$Wxu = (A - F)' Q B$$

$$Wxd = (A - F)' Q G$$

$$Wdu = G' Q B$$

Next, the derivation follows the standard steps: append the dynamical equations of the plant to the cost function as a constraint, integrate by parts, and take the first variation in cost with respect to the control, state, and adjoint variable [20,21]. Variations in the input variable d(t) are not allowed because it is external to the system, and can be thought of as an unknown disturbance. This results in three equations relating the input d(t) and the control u(t) to the state x(t) and adjoint state l(t):

$$\dot{l} = - Wxx\, x - Wxu\, u + Wxd\, d - A'l$$

$$u = Wuu^{-1} \{ - Wxu'x - B'l + Wdu'd \}$$

$$\dot{x} = A\, x + B\, u \qquad (3.6)$$

and upon substituting for u(t):

$$\begin{vmatrix} \dot{x} \\ l \end{vmatrix} = \begin{vmatrix} [\, A - B\, Wuu^{-1} Wxu \,] & [\, -B\, Wuu^{-1} B' \,] \\ [\, -Wxx + Wxu\, Wuu^{-1} Wxu' \,] & [\, -A' + Wxu\, Wuu^{-1} B' \,] \end{vmatrix} \begin{vmatrix} x \\ l \end{vmatrix} + \begin{vmatrix} [\, B\, Wuu^{-1} Wdu' \,] \\ [\, Wxd - Wxu\, Wuu^{-1} Wdu' \,] \end{vmatrix} \begin{vmatrix} d \end{vmatrix} \qquad (3.7)$$

Comparison with the derivations in [20,21] will show that the only difference here is in the extra term due to the model input. As was done for the homogeneous equation of [20,21], we will assume the solution for the adjont variable to be a linear function of the state variable, but we'll also include an inhomogeneous part due to the model input:

$$l(t) = P(t)\, x(t) - S(t)\, d(t) \qquad (3.8)$$

which upon taking the derivative becomes:

$$\dot{l}(t) = \dot{P}(t)\, x(t) + P(t)\, \dot{x}(t) - \dot{S}(t)\, d(t) \qquad (3.9)$$

Since the model input is a measurable but unpredictable quantity, the best estimate of its derivative is zero; therefore it does not appear in equation (3.9) [19]. Substituting into (3.7) gives:

$$\begin{aligned} &\dot{P}x + P[\, A - B\, Wuu^{-1} Wxu' \,]x + P[\, -B\, Wuu^{-1} B' \,]Px - PSd \\ &+ P[\, B\, Wuu^{-1} Wdu' \,]d - \dot{S}d = [\, -Wxx + Wxu\, Wuu^{-1} Wxu' \,]x \\ &- [\, A - B\, Wuu^{-1} Wxu' \,]'Px + [\, A - B\, Wuu^{-1} Wxu' \,]'Sd \\ &+ [\, Wxd - Wxu\, Wuu^{-1} Wdu' \,]d \end{aligned} \qquad (3.10)$$

If the cost were truly at a minimum, then the above equation must be true regardless of the variation in x or the value of d. Thus, we can separate out all the dependence upon these two quantities, giving two separate equations:

$$\begin{aligned} -\dot{P} = {} & P[\, A - B\, Wuu^{-1} Wxu' \,] + [\, A - B\, Wuu^{-1} Wxu' \,]'P \\ & - [\, -Wxx + Wxu\, Wuu^{-1} Wxu' \,] + P[\, -B\, Wuu^{-1} B' \,]P \end{aligned} \qquad (3.11)$$

$$\begin{aligned} -\dot{S} = {} & [\, A - B\, Wuu^{-1} Wxu' \,]'S + P[\, -B\, Wuu^{-1} B' \,]S \\ & - P[\, B\, Wuu^{-1} Wdu' \,] + [\, Wxd - Wxu\, Wuu^{-1} Wdu' \,] \end{aligned} \qquad (3.12)$$

and the control is then:

$$u = -Wuu^{-1} [\, Wxu' + B'P \,]x + Wuu^{-1} [\, Wdu' + B'S \,]d \qquad (3.13)$$

Several observations concerning the form of these equations can be made. First, the Riccati equation for the state cost matrix, (3.11), is unchanged from the standard form [16]. The only differences are the actual values for the cost matrices. From (3.4), one may note that these cost matrices are independent of G, the input matrix in the model dynamics. Second, equation (3.12) for the variation of S, the state and model input cross-cost, is linear and depends explicitly on both the G matrix and the solution to the Riccati equation (3.11). And finally, the expression for the optimal control shows a feedback gain for the states that depends on P and a feedforward gain for the model input that depends on S. Only the feedforward gain is influenced by the choice of the model input matrix G.

Since the homogeneous equations were shown to have an efficient "spectral" solution that could be calculated after at most two integration passes over the fundamental period [16,22], it would be very desirable to develop a similar technique for handling the calculation of the feedforward gains. Fortunately, one was found by incorporating a combination of the method of [22] with the algorithm for initial conditions of [23].

Following the lead of [22], if one represents equation (3.7) in the form:

$$\begin{vmatrix} \dot{x} \\ l \end{vmatrix} = \begin{vmatrix} A(t) \end{vmatrix} \begin{vmatrix} x \\ l \end{vmatrix} + \left|\begin{array}{c} M(t) \\ \hline N(t) \end{array}\right| \qquad (3.14)$$

one can numerically compute this system's (2nx2n) augmented state transition matrix, where n is the dimension of both x(t) and l(t) [24]. Call this matrix B(t,t0). If one solves for the eigenvalues and eigenvectors of the resulting Floquet transition matrix for this 2n system, and then separates them into stable and unstable modes, the steady-state periodic solution to the Riccati equation of (3.11) can be shown to be:

$$P(T) = T21(T)\, T11(T)^{-1}$$

$$\text{and:}\quad P(t+T) = [\, B21(t,0)*T11(T) + B22(t,0)*T21(T) \,] * [\, B11(t,0)*T11(T) + B12(t,0)*T21(T) \,]^{-1} \qquad (3.15)$$

where the matrices T11 and T21 represent the (2nxn) eigenvectors associated with the stable modes of the FTM.

This is only the solution to the homogeneous part of (3.14). One then solves for the (2nxm) particular periodic solution of (3.14) using [23]; call the transpose of this (2nxm) time-varying matrix [Xp' | Lp'], where m is the dimension of the model input. Then (with considerable hindsight) one has the solution to the cross-cost matrix S as:

$$S(t) = -Lp(t) + P(t)\, Xp(t) \qquad (3.16)$$

Verification of this result can be done by taking the derivative of (3.16), substituting the two equations of (3.14) and the Ricatti equation of (3.11), and comparing the result with (3.12).

This process can be improved upon by combining the solution for the particular form of (3.14) with the procedure for determining the (2nx2n) state transition matrix by integrating the augmented matrix:

$$Z(t)_{(2nx(2n+m))} = \left|\begin{array}{c|c} B(t) & \begin{array}{c} X(t) \\ \hline L(t) \end{array} \end{array}\right| \qquad (3.17)$$

with the initial conditions:

$$B(0) = I_{(2nx2n)}, \quad X(0) = L(0) = 0_{(nxm)}$$

over a modified form of (3.14):

$$\dot{Z}(t) = A(t) * Z(t) + \left|\begin{array}{c} M(t) \\ \hline N(t) \end{array}\right| \qquad (3.18)$$

where I represents the identity matrix. After one cycle of integration, one has:

$$Z(T) = \left|\begin{array}{c|c} FTM_{(2nx2n)} & \begin{array}{c} X(T)_{(nxm)} \\ \hline L(T)_{(nxm)} \end{array} \end{array}\right| \qquad (3.19)$$

Then from [23] one obtains the initial conditions for the particular solution as:

$$\begin{vmatrix} Xp(0) \\ Lp(0) \end{vmatrix} = \begin{vmatrix} I_{(2nx2n)} - FTM_{(2nx2n)} \end{vmatrix} \begin{vmatrix} X(T) \\ L(T) \end{vmatrix} \qquad (3.20)$$

Upon finding the eigenvalues and eigenvectors of the FTM, one need only preform a second integration pass over equation (3.18) to solve for the matrices P(t) and S(t). In this way, the number of integration passes can be reduced by one, a considerable saving for high-order periodic systems.

3.3 Numerical Results for Implicit-Model-Following

In order to see the effects of a model-following design on a periodic system using a constant-coefficient model, the following scalar example was used:

$$\dot{x}(t) = a(t)\, x(t) + b(t)\, u(t)$$

$$\dot{x}_m(t) = f\, x(t) + g\, d(t)$$

where: $a(t) = -1. + \cos(t)$
$b(t) = 1.$
$f = -1.$
$g = 1.$

As the weighting matrix Q was varied, the following behavior in the poles was observed (with R=1.0):

Q	F-plane pole	L-plane pole
0.	1.868e-03	-1.0
.01	1.822e-03	-1.004
0.1	1.552e-03	-1.029
1.0	1.231e-03	-1.066
3.0	1.392e-03	-1.047
10.	1.642e-03	-1.020
100.	1.839e-03	-1.010
(R=0.)	1.867e-03	-1.000

This behavior is typical of model-following designs for periodic plants that posess enough controllability to allow an exact model matching. This can be seen in figure 4, where the gain function for the case of no control penalty (R=0.) is plotted. The curve is a perfect cosine function, which exactly cancels the system's periodicity, as can be seen in figure 5, where the open- and closed-loop eigenvector are shown.

For the helicopter rotor operating at a high-advance ratio, however, exact model matching is not always possible. A good example of this can be seen in figure 6, where one of the rotor feedback gain functions for an advance ratio of 1.4 is plotted for increasing values of state penalty, Q. Even though the flapping dynamics represent a higher-order system, the fact that the equations are written in a control-canonical form (meaning the states are just the various time derivatives of the displacement) reduces the model-matching cost term in (3.3) to a scalar. The most striking feature of this plot is the manner in which the gain values approach singularities on the retreating side of the rotor azimuth. This can be explained by referring to the control power term in the equation of motion (2.1) in figure 3. At this high advance ratio, the control term can be seen to cross through zero twice on the retreating side. Thus, in order to cause the closed-loop system

$$\dot{x} = [\, A(t) - B(t)\, K(t) \,]\, x + [\, B(t)\, Kff(t) \,]\, d \qquad (3.20)$$

to act like a constant-coefficient system, the gain would have to become infinite to cancel the periodicity of A(t) at that particular azimuth angle.

This result raises the question of controllability for linear periodic systems. [25] defines several types of controllability, all of which are rather difficult to assess without substantial computational resources. The strongest level is "uniform controllability", where the state can be driven through impulsive inputs in an infinitesimal time to another desired state at any instant over some specified time interval. Clearly the above example falls short of this ideal, since it is uncontrollable at two specific azimuth locations on the retreating side. All is not lost, however, as these two points are isolated instants and not continuous stretches of time, and thus limit this example to a case of "total controllability". Quite reasonable results can be achieved even for this case, as can be seen by the plot of the real part one of the eigenvectors of the closed-loop system in figure 7. Significant reductions are realized in the system's periodicity for moderate levels of model-matching cost and feedback gains.

The closed-loop pole locations for fixed cost and varying advance ratio are shown in figures 8a for the Laplace-plane and 8b and 8c for the Floquet plane. It is evident that the effect of increasing advance ratio is diminished for larger cost values, as the poles do not shift nearly as much as for previously considered controller designs. This is indeed an attractive feature for helicopter rotor control, and thus this approach was used for the controllers demonstrated in the following sections of this paper.

4. Observer Design and Parameter Identification

4.1 Introduction to Observer Theory

Most control system engineers, if they have produced a design using modern control theory state-space concepts, have had to wrestle with the following problem upon completion of their choice of a candidate regulator: not all the state variables of the system are available for measurement. The most frequent situation is that just a few are measurable, and even these may be constrained to be measurable only in certain linear combinations. This general situation can be represented by the linear time-varying set of equations:

$$\dot{x}(t) = A(t)\, x(t) + B(t)\, u(t) \qquad (4.1.1)$$

$$y(t) = C(t)\, x(t) + D(t)\, u(t) \qquad (4.1.2)$$

where x(t) is the n-dimensional state vector, u(t) the m-dimensional control vector, and y(t) is the l-dimensional measurement vector. This predicament is not unsolvable within the context of the theory, but the solution is often the most complex element of the controller design process.

One obvious way to generate the estimates of the state variables is to integrate the equations (4.1.1-2) forward in time. This simplistic approach is, in general, doomed to failure because it requires both an exact representation of the actual system dynamics and the knowledge of the initial conditions of the state variables. Such a technique makes no use of the current value of the measurement and as such becomes susceptible to any and all errors introduced through disturbances acting on the actual system. Furthermore, if the system being modelled is unstable, these errors are likely to grow without bound.

Observer theory incorporates the concept of negative feedback to force the errors in the state estimates to approach zero exponentially with time. This is done by driving a model of the system with an input proportional to the difference between the actual measurements and the predicted values based on the current state vector estimate. That is, we formulate the system (for the continuous-time case) as:

$$\dot{\hat{x}}(t) = A(t)\, \hat{x}(t) + B(t)\, u(t) + K(t)[\, y(t) - C(t)\, \hat{x}(t) \,] \qquad (4.1.3)$$

where:

$$y(t) = C(t)\, x(t) \qquad (4.1.4)$$

If we define the estimation error as:

$$e(t) = \hat{x}(t) - x(t) \qquad (4.1.5)$$

then the error is governed by:

$$\dot{e}(t) = [A(t) - K(t)C(t)]\, e(t) \qquad (4.1.6)$$

The choice of this proportionality constant K(t) determines the speed in which these errors are reduced, and can be selected using any of several methods, the most popular being the Kalman Filter. But perhaps the most important result from observer theory is the fact that use of the state estimates instead of the actual states for feedback does not alter the closed-loop stability of the system. The poles of the combined observer-controller are those of the state-feedback controller, plus those of the observer error dynamics. The only consequence of using an observer is often a deterioration of the transient response of the complete closed-loop system. This result is called the "separation principle" and allows one to perform independent designs of the state feedback gains and the observer dynamics.

A Kalman Filter is a technique for producing the best linear estimate of a state vector given the a-priori knowledge of the random processes perturbing the system to be observed, the knowledge of the structure of the noise corrupting the measurements, and the exact model of the plant dynamics relating the various physical quantities. It can be shown that the formulation of the Kalman Filtering problem is "dual" to that of the optimal controller problem, in that the optimization equations only differ through a sign change, representing a forward propogation of time instead of a reverse one [21]. The proportional feedback gains on the measurement errors (known as "residuals") are computed as representing the best tradeoff between reduced sensitivity to sensor noise and increased ability to quickly track changes in the state vector.

The requirements for implementing a full Kalman Filter for a complex plant are often too severe in terms of required a-priori knowledge and system order to warrant its use in a feedback controller design. In the context of helicopter rotor control, a full-blown Kalman Filter would necessitate modelling several rotor blade modal degrees of freedom along with the highly complex dynamics of the rotor wake, including any effects of gusts, dynamic inflow, returning tip vortices, and so on. Such a model, even if made reasonably accurate, would be so complex and costly as to render its use in a control design impractical. Thus, techniques to generate a simpler, sub-optimal estimate of the state vector would be very valuable.

4.2 Observers for Rotor Control

The solution presented in the following pages to this problem arose out of the need to adequately describe the sensor complement present in the Individual-Blade-Control model rotor system. The two available sensors for out-of-plane blade motion detection are a tip-mounted accelerometer, with its sensitive axis perpendicular to the

blade surface, and a blade root angle transducer mounted at the flapping hinge. As can be seen in figure 9, this particular choice of location for the accelerometer results in its output being proportional to out-of-plane position as well as acceleration, due to its orientation in a centrifugal force field. If the rotor blade motion is described by an infinite series of time-varying modal displacements, then the ratio of these two effects is determined by the mode shape slope and displacement at the tip for each blade mode considered. That is, if the out-of-plane displacement is:

$$z(t) = \sum_{i=1}^{inf} \eta_i(x)\, g_i(t) \quad , \quad x = r / R \qquad (4.2.1)$$

then the accelerometer senses:

$$accel(t) = \sum_{i=1}^{inf} \left\{ \eta_i(x) \frac{d^2 g(t)}{dt^2} + r\,\Omega^2 \frac{d\eta_i(x)}{dr} g_i(t) \right\} \qquad (4.2.2)$$

If we restrict ourselves to considering only the first out-of-plane mode of the blade, namely, rigid flapping, then this infinite sum is truncated at the first term, and we have a sensor that gives a signal that is a linear combination of flapping position and acceleration. Looking back at equation (4.1.2), one notices that the standard form for representing a sensor's output is as a linear combination of states and controls, but it is immediately apparent that this has been complicated by using an accelerometer. Since modal acceleration is not a state variable but a time derivative of a state, one must represent the sensor by incorporating the system dynamics in the observation matrices. Thus, for an accelerometer that senses the combination:

$$accel(t) = H1\, x(t) + H2\, \dot{x}(t) \qquad (4.2.3)$$

then this can be reconfigured to be:

$$accel(t) = H1\, x(t) + H2 \{ A(t)\, x(t) + B(t)\, u(t) \} \qquad (4.2.4)$$

or,

$$accel(t) = \{ H1 + H2\, A(t) \}\, x(t) + \{ H2\, B(t) \}\, u(t) \qquad (4.2.5)$$

This is indeed an unfortunate situation. Whereas before we had a sensor that was related to a combination of the state vector and its time derivative, now the representation of the sensor content is directly dependent upon the description of the system dynamics, including all its elements of periodicity and variation with flight condition. An observer or Kalman filter design based upon this set of equations would be complex indeed! Fortunately, there are techniques to circumvent such difficulties, two of which are described in the next section.

4.3 Incorporation of Accelerometers into Observer Design

For a lumped-parameter system, if one knows the lumped mass and inertial properties of a system incorporating an accelerometer sensor, it becomes possible to solve for the applied forces and moments acting on it. These include any control actions or disturbances of the plant, and thus could supply a predictive quality, or "lead", for any observer using an accelerometer in the estimation task. It is with this concept in mind that the following approach was developed: the acceleration is considered to be a deterministic input into the system, which can be accurately measured.

If one is willing to assume that process noise dominates the stochastic elements present in the system, we can treat the acceleration as a measurable, "deterministic" quantity and use it to drive a system modelled by the equations:

$$\frac{d}{dt}\begin{vmatrix} x \\ \dot{x} \end{vmatrix} = \begin{vmatrix} 0 & 1 \\ 0 & 0 \end{vmatrix} \begin{vmatrix} x \\ \dot{x} \end{vmatrix} + \begin{vmatrix} 0 \\ 1 \end{vmatrix} accel(t) + \begin{vmatrix} 0 \\ 1 \end{vmatrix} w(t) \qquad (4.3.1)$$

$$y(t) = \begin{vmatrix} 1 & 0 \end{vmatrix} \begin{vmatrix} x \\ \dot{x} \end{vmatrix} + \begin{vmatrix} 1 \end{vmatrix} v1(t) \qquad (4.3.2)$$

where $w(t)$ represents a zero-mean gaussian process noise, and $v1(t)$ represents a zero-mean gaussian sensor noise.

Trading off the values of the process noise covariance with the position sensor covariance produced a design with a gain matrix of:

$$K = \begin{vmatrix} 14.14 \\ 100.0 \end{vmatrix}$$

and observer poles of $(-7.07, 7.07j)$. To test this design, a digital simulation of a higher-order system was run with non-zero initial conditions, using this observer to compute the state estimates. The tracking performance of this observer design is illustrated in figure 10b, where the velocity estimate is almost indistinguishable from the actual system response in figure 10a. This observer structure would also appear to be a good candidate for use in a feedback controller design. The advantage of this approach is a reduction in observer hardware without a deterioration in performance.

4.4 Observing the States of a Time-varying Plant

Since the ultimate purpose of these observer designs is to generate state estimates of a time-varying rotor system, it seems most appropriate to test them against the actual values present in such a complex environment. This validation procedure, however, is complicated by the fact that the M.I.T. Individual-Blade-Control model rotor system has no means of measuring flapping rate -- if it did, the need for an observer would then not exist! Instead, an analog simulation of the full out-of-plane rigid flapping equations of motion was built up from operational amplifiers and integrated circuits, as outlined in Section 5, to serve as a test bed for both observer design and controller implementation. This simulation includes the effects of reversed flow and provides as output several voltages representing all the rotor states, controls, sensor outputs, and periodically-varying equation coefficients present in the linearized small-displacement flapping equation of motion.

The second-order observer designed in the previous section was also built from analog hardware and connected to the "sensor" outputs of the analog simulation. These "sensor" signals represent the outputs from the flap strain gauge and the tip accelerometer. Since the observer was designed on the assumption that the acceleration was directly measurable, the centrifugal component of flapping displacement had to be subtracted out of the simulated tip accelerometer signal prior to incorporation into the observer structure. This by no means presents any difficulty, as the portion of the tip accelerometer signal multiplying flapping displacement is time-invariant, being neither a function of azimuth nor flight condition.

Just as was done previously for the digital computer simulation trials, the flapping rate signal was selected as the means of comparison for evaluating the observer's tracking performance. In order to provide adequate testing of transient conditions, a square-wave was fed into the pitch signal of the analog simulation, and the resulting flap rate and flap rate estimate were observed. These signals, along with the once-per-revolution timing pulse, are plotted in figure 11, representing a rotor operating at an advance ratio of 1.14. The results are similar for all other advance ratios and all other types of external forcing functions: the flapping rate signal is essentially perfectly reconstructed. There is no doubt that use of this quantity in a state-feedback controller would produce satisfactory results, as it tracks even small detailed fluctuations in state due to the pitch forcing.

This most fortunate result has interesting implications. Since a time-invariant observer incorporating acceleration measurements is capable of adequately observing the state of a complex, time-varying plant, one then wonders if similar techniques are equally applicable to nonlinear or even nonlinear and time-varying systems as well. Of equal interest is how to estimate additional modal degrees of freedom using the same type of sensor complement, and how to attribute the measurement residuals to the various modes.

This latter question appears to be solvable using the second method outlined above, that of forcing a "double-integral" plant with a modal acceleration and correcting its output with a position measurement. Since all that is really needed for such an application is an accurate measurement of the particular modal acceleration and displacement, one does not even need to simultaneously estimate the dynamics of the lower-order modes. This can be best seen if one considers the modal content of each of the sensors.

For a system of, say, two modes instead of one, each accelerometer will measure some linear combination of the modal accererations that will depend upon its location on the structure. Thus, if two accelerometers are located at different points on the structure, their outputs can be combined so as to solve for each modal acceleration, provided their outputs do not also contain modal position information as well, such as in equation (4.2.2). This same argument holds for requiring two position sensors in order to solve for the two modal displacements. For the case of the Individual-Blade-Control rotor, since the accelerometers contain modal displacement information as well, one can add two additional accelerometers to the previous complement of a tip accelerometer and root angle transducer, and still solve for the two modal accelerations and displacements uniquely.

Once one has the individual modal acceleration and displacement information, one need merely design an observer such as that of (4.3.1-2), with a bandwidth picked to be sufficiently faster than the mode's natural frequency. Unlike a conventional Kalman Filter, there is no need to estimate the lower modal states, and thus the observer need only be of order two for any mode desired. However, we have reduced the complexity of the Kalman Filter approach, with all its possible time-variation and higher order, at the expense of additional sensors. For some plants, this may not be justifiable, but for helicopter rotor control, the advantages appear to outweigh the additional cost of more sensors.

4.5 Periodic System Parameter Identification

Even with perfect measurements of the system state variables, any controller design based on modern techniques would be doomed to failure if the mathematical model for the plant being controlled were grossly in error. This applies equally for periodically time-varying systems as well as for time-invariant ones. Fortunately, given the accurate state variable estimation results of the previous section, extracting the periodic coefficients of the flapping equation (or for that matter, any reasonably uncoupled modal response) can be reduced to a basic least-squares procedure. The technique described below is equally applicable to any other type of time-varying dynamics, provided that the time variation of the coefficients can be described using weighted linear combinations of orthogonal time functions.

Given the flapping equation of the rotor in the rotating frame as:

$$\ddot{\beta} + A1(\psi)*\dot{\beta} + A0(\psi)*\beta = B0(\psi)*\theta \qquad (4.5.1)$$

where the primes indicate differentiation with respect to azimuth angle, the periodic coefficients A1, A0 and B0 can be represented as an infinite sum of trigonometric functions of azimuth according to:

$$A1(\psi) = A10 + \sum_{n=1}^{inf} \{ A1cn*\cos(n\psi) + A1sn*\sin(n\psi) \}$$

$$A0(\psi) = A00 + \sum_{n=1}^{inf} \{ A0cn*\cos(n\psi) + A0sn*\sin(n\psi) \}$$

$$B0(\psi) = B00 + \sum_{n=1}^{inf} \{ B0cn*\cos(n\psi) + B0sn*\sin(n\psi) \} \qquad (4.5.2)$$

If these expressions are substituted into equation (4.5.1) and the resulting products of state variables and coefficient harmonics are expanded, one obtains (after solving for the acceleration):

$$\begin{aligned}\ddot{\beta} = [\ &\beta' + \beta^{c}\cos(\psi) + \beta^{s}\sin(\psi) + \beta^{c}\cos(2\psi) + \\ &\beta^{s}\sin(2\psi) + \beta^{c}\cos(3\psi) + \ldots + \beta + \beta*\cos(\psi) + \\ &\beta*\sin(\psi) + \beta*\cos(2\psi) + \beta*\sin(2\psi) + \ldots + \\ &\theta + \theta*\cos(\psi) + \theta*\sin(\psi) + \theta*\cos(2\psi) + \\ &\theta*\sin(2\psi) + \theta*\cos(3\psi) + \ldots\ ] * \\ [\ &-A10\ -A1c1\ -A1s1\ -A1c2\ -A1s2\ -A1c3\ \ldots\ -A00\ -A0c1 \\ &-A0s1\ -A0c2\ -A0s2\ \ldots\ B00\ B0c1\ B0s1\ B0c2\ \ldots\ ]^{T}\end{aligned} \qquad (4.5.3)$$

This equation is linear in the parameters representing the harmonics of the periodic coefficients. Since the observer structure outlined in the previous section provides accurate estimates of the states and modal acceleration, if we measure the control input (as we must) we can treat these harmonics as the unknowns in our problem. This then gives us a linear equation in as many unknowns as we care to estimate, corresponding to the number of harmonics desired to represent the periodic coefficients.

Since this equation is valid over any azimuth angle, substitution of the rotor states, control input and accelerations into (4.5.3) for many different azimuth locations will provide as many or more equations than unknowns that are needed to solve for these coefficients uniquely. Due to the complex nature of the rotor wake, a least-squares approach was used in order to reduce the variance in these estimates due to process noise. If one rewrites (4.5.3) in vector form and solves for the error between the measured acceleration and that predicted from the coefficient values, one has:

$$E = Y - [\ dY/dA\ ]*A \qquad (4.5.4)$$

where: E is a (mx1) vector of prediction errors
Y is a (mx1) vector of measured accelerations
[dY/dA] is a (mxn) matrix of products of states and controls with sines and cosines
A is a (nx1) vector of harmonics of coefficients
m is the number of data points (azimuth locations) considered
n is the number of harmonics to estimate

and to minimize the sum-squared error in the estimate, one takes the first derivative of the square of (4.5.4) and equates it to zero. This results in the traditional "normal equations":

$$A = \{ [\ dY/dA\ ]^{T} [\ dY/dA\ ] \}^{-1} * [\ dY/dA\ ]^{T} * Y \qquad (4.5.5)$$

In order to reduce the effects of unmodelled accelerations or sensor noise, many data points should be used. This will cause the data-dimension (m) of the vector Y and of the matrix [dY/dA] to grow to an unacceptable size in terms of storage requirements unless the following steps are taken. Since the dimension m gets "absorbed" in the inner products of [dY/dA] with itself and in [dY/dA] with Y, one can treat these two products as "buffers" of dimension (nxn) and (nx1), and sum each new data point vector into them according to:

$$A = U^{-1} * V\ ;\quad U = \sum_{i=1}^{m} [\ dY_i/dA\ ]^{T} [\ dY_i/dA\ ]$$

$$V = \sum_{i=1}^{m} [\ dY_i/dA\ ]^{T} Y_i \qquad (4.5.6)$$

where i represents a single azimuth angle. It should be noted that U is formed by summing outer products of sensitivity vectors. In this way the largest storage dimension is just n, the number of coefficient unknowns.

To test this approach, a computer program was written [16] that would solve for the periodic coefficients given the desired number of harmonics and the data files of rotor state, acceleration and control input. The analog simulation described in Section 5 was once again used to generate time histories for such testing purposes, and the results can be seen in figures 12a, 12b and 12c. The analog model was excited using a swept-sinewave source on the pitch simulation channel, and the outputs representing flap and tip accelerometer signal were fed into the second-order observer to generate flapping acceleration and rate estimates. These signals as well as the actual coefficient voltages were fed into the PDP-11/03 computer, digitized, and stored as data files. The estimated coefficients compare quite favorably with the actual measured values, indicating the validity of this technique.

5. Experimental Apparatus

5.1 Analog Simulation

In order to both test concepts and validate controller designs, it was felt necessary to construct an electronic circuit that would produce signals much like that of the Individual Blade Control rotor in the wind tunnel. This circuit card was designed to have coefficients that were periodic functions of time similar to those of the actual model. During the early stages of design it was found that by incorporating several voltage multiplication integrated circuits (IC's) it would indeed be possible to simulate the single flapping mode equations. Through a series of comparitor IC's described below, it was even possible to include the effects of reversed flow in the coefficients.

Construction of the simulation was done on a single plug-in card that was compatible with the instrumentation rack used in the actual rotor signal processing. This was initially intended to allow its use as a dynamic element within a full-blown Kalman filter state estimator, although this later proved to be unnecessary. The rack mounting provided the card's supply voltages, and all other voltages representing rotor states and coefficients were brought to a central terminal strip at the front of the instrument cabinet.

The layout of the circuit was done in four segments: timing generation, coefficient computation, coefficient selection, and blade flapping simulation. This division was used in order to reduce the parts count of the simulation as much as possible. As was explained in Section 2, the rotor blade passes through at least two and possibly three different regions of tangential airflow as it rotates about the shaft. The aerodynamic moments created about the flapping hinge for these cases of normal, mixed, and reversed flow can be expressed analytically, although each coefficient formula is only valid for that particular region. In order

to accurately express this periodic variation of coefficients analytically for the entire azimuth, many harmonics would have to be retained. This would create the need for an unacceptably large number of IC's, and thus the design incorporated an analog switching network to select the appropriate equation coefficients for the current azimuth angle of the simulation.

Inspection of the coefficient equations in Section 2 reveals that, for the case of no hinge offset, each region's variation with azimuth angle is constrained to polynomials in the product of advance ratio and the sine of the azimuth angle. Thus, given an input sinusoid with amplitude proportional to advance ratio, one may readily generate the higher terms of the polynomial using analog multiply IC's. Weighted values of these products of sinusoids were then combined using standard operational amplifiers to produce voltages that corresponded to the expressions valid for each flow region. These were fed simultaneously to a set of *analog multiplexers that would select whichever of the three* voltages (three for each of three coefficients) was appropriate at the particular azimuth angle of the simulation.

Timing for the circuit was accomplished using a commercially available function generator IC, capable of oscillating at a frequency set by external passive components. Outputs of this IC included a fixed-amplitude sine wave and square wave. Since a cosine wave was also needed for the coefficient generation (in the aerodynamic *flapping spring term), a constant-amplitude phase lead* network was built to shift the sine wave signal by 90 degrees. As such a network's phase shift is not independent of frequency, it became necessary to fix the oscillator frequency to a specific value. This was set to 5 Hertz in order to match the rotation speed of the actual model rotor.

The oscillator's sine wave was input to an amplifier to vary its amplitude according to an "advance ratio" set by a dial potentiometer on the front panel. Since the transition between different flow states of the blade (and hence its *coefficient expressions) is directly dependent upon this* value, this was also used as a control voltage for input to the comparitor IC's that generated the select voltages that drove the multiplexers. This same amplified sinusoid was used for the polonomial term generation as described earlier.

Finally, the blade dynamics were simulated using standard op-amps as with most analog computers, but the coefficients for the system were taken from the outputs of the multiplexers. These were fed into another set of analog multiply IC's in order to permit time-varying dynamics. The *integrators in the simulation were scaled to keep these* coefficient voltages to values well within those of the power supply. Also, the voltages representing the flap angle and flap acceleration were combined to simulate the blade tip accelerometer signal. This voltage, along with the voltages representing the rotor blade flap angle, flap velocity, flap acceleration, pitch angle, coefficient values, sine and cosine waves and the square wave timing signal, were all brought to a terminal strip on the front panel. This arrangement allowed rapid evaluation of candidate control *laws as well as verification of the response of the modal* state estimator.

5.2 Model Rotor Hardware and Instrumentation

The Individual Blade Control model rotor used at M.I.T. is a four foot diameter single-bladed rotor with two opposing counterweights. The blade flapping hinge is offset slightly from the shaft centerline and attached to a fully articulated hub incorporating a spherical bearing arrangement, permitting *flap, lag and pitch degrees of freedom to have coincident* axes. A steel flexure attached to this hub allows measurement of blade flap and pitch angle through a set of strain gauges mounted on its surface. Mounted within the blade structure at the tip is a miniature accelerometer, with its sensitive axis oriented perpendicular to the blade surface. This location permits measurement of both flapping displacement as well as flapping acceleration, as described in Section 4. Blade pitch control is achieved through a series of pushrods and gears driven by a shaft mounted DC motor, with a servo loop closure formed around the pitch *angle strain gauge and the motor's integral tachometer* signal.

The model rotor hub geometry and pitch actuator were unchanged from that used for a previous gust-response test [1]. However, since the rotor no longer needed to align with external gust generators, a new housing was constructed for the slipring assembly at the end of the shaft that permitted a vertical shaft orientation. This eliminated spurious once-per-revolution gravity effects on the tip accelerometer sensor allowing operation at lower rotation speeds on an *existing rotor test stand within the M.I.T.* acoustic wind tunnel. Figure 13 shows the single-bladed model rotor and rotor stand, along with a simulated fuselage forebody attatched to the upstream side.

While the rotor hardware was unchanged from the gust alleviation tests, the instrumentation complement for acquiring, displaying and processing the wind tunnel data was vastly improved. Figure 14 details the signal paths from the rotor sensors to the amplifiers, signal conditioners and data recorders used in the experiment. Central to the experiment was the signal conditioning rack. This unit contained the pitch and flap strain gauge differential amplifiers, the tip accelerometer amplifier, the servo motor current amplifier and power supply along with the servo feedback controller card, the instrumentation amplifier power supply, and a set of timing circuitry capable of measuring rotor rotation and supplying a squarewave at rotation frequency and another squarewave at an integer multiple of rotation frequency.

Attached to this rack were an FM tape recorder for saving analog voltage data; a Nicolet 660B dual-channel spectrum analyzer for transfer function, power spectrum and quick-look data analysis; a set of oscilloscopes for rotor sensor monitoring; and a PDP-11/03 minicomputer for digital data collection and storage. This same computer was used to generate the synchronized periodic feedback gains and control commands, and because of the time-critical nature of this task, the computer data collection for closed-loop tests was done off-line using the signals collected on the FM tape recorder.

A typical experiment run consisted of the following set of procedures. First the pitch servo was energized and the rotor brought up to rotation speed using the hydraulic drive system mounted in the tunnel. Then the wind tunnel speed was increased while the rotor collective pitch was adjusted to minimize the flapping response of the blade. A swept-sinewave source was fed into the blade pitch command summing junction, and a set of open-loop analog data was stored on the four-channel FM tape recorder, consisting of the 1/rev timing squarevave, the excitation signal, the flapping gauge signal, and the tip accelerometer voltage. After a record of sufficient length was captured, the appropriate program was run on the computer to generate the periodic gains and output the control commands through a digital-to-analog converter board to the pitch servo summing junction. The computer used the state estimates from the analog observer as its input, and comprised the feedback controller circuitry. A digital structure was used, as the computation speed required for the multiplication operations was within the capability of the computer.

The same four voltages were then stored on the tape recorder, and the spectra of the pitch and flap channels were monitored to observe the effect of controller action on the system. Upon tunnel and rotor shut-down, the cables were swapped and the tape recorder was played back into the signal conditioning rack to generate the timing pulses for the analog-to-digital converter board. These same signals were fed into the observer circuitry, and the whole complement of sensor and state estimate data was fed through an eight-channel low-pass anti-aliasing filter box and into the computer. The data files resulting from the digitized data were used for subsequent analysis and parameter identification experiments, the results of which appear in Section 6.

6. Experimental Results

6.1 Introduction

Classical representations of system dynamics, such as transfer functions, cannot easily be used to describe systems with periodic coefficients. Familiar concepts such as phase and gain margin are not applicable since these systems exhibit responses at several frequencies to a single excitation frequency. Because of this, a higher level of sophistication is necessary to quantify the character of a periodic plant. In Section 4, a unique direct parametric representation was shown to be possible, due to the relative ease of reconstruction of the missing state variables. This same technique will be used in this Section. By comparing the identified periodic coefficients for open- and closed-loop time response tests on the experimental apparatus, we will be able to judge the effect of a particular control law on system performance.

Prior to actual wind tunnel tests of the rotor model, a series of control laws were tested on the analog simulation. All the closed-loop controller designs were of model-following structure, with the model possessing time-invariant dynamics. Thus, the closer the identified coefficients approached a constant value, the more the closed-loop system behaved like the desired model. The next two parts of this Section illustrate exactly this behavior for both the simulation and the actual rotor.

6.2 Analog Simulation Results

The test procedure for the analog simulation was very similar to that for the wind tunnel model as described in Section 5. First, a swept-sinewave excitation was fed into

the pitch channel of the simulation, and this signal as well as the simulated flap channel and tip accelerometer channel were stored on an FM tape recorder. After a sufficient amount of data was collected, these signals were played back as input to the observer. These signals, as well as the observer's estimates of simulated flap rate and acceleration, were then brought to the 8-channel anti-aliasing filter box, digitized and stored in a data file in the computer. After several of these files were collected, the coefficient regression routine was run on them, and the fitted values as well as statistical goodness-of-fit parameters were printed on a hard-copy terminal. Then the digital controller was turned on and the entire process repeated. A plot of a typical data file for use in the coefficient identification process can be seen in figure 15 It should perhaps be noted that the regression only uses four of these channels directly: the excitation signal, and the flap, flap rate and flap acceleration signals.

In order to provide a suitably harsh test environment, the simulation was run at an effective "advance ratio" of 1.4, corresponding to the highest advance ratio to be experienced by the model in the wind tunnel. This test condition provided the highest level of periodicity present in the system to be controlled, and hence the largest gains and greatest controller effort required. Inspection of figures 16a, 16b and 16c reveal that this simulation operating point posed no problem for the controller, as the periodicity can be seen to be reduced for the control power, spring and damping terms of the system.

Closer inspection of these figures shows that in some cases the mean levels of the parameters were reduced. This is not a destabilizing effect of periodic control, but instead a consequence of the particular model chosen for the performance function; a model with higher damping would have produced higher damping levels in the closed-loop system. The limiting factor in model-following ability appears to be associated with the controllability issue addressed earlier. Systems that do not posess full controllability over all azimuth locations cannot be made to match a model perfectly.

As a final check of the reduction of periodicity in the system, a single frequency excitation was fed into the simulation for both the open- and closed-loop cases. The resulting input and output power spectra are shown in figures 17a and 17b. Not only is the subharmonic just below the fundamental (at 5Hz) reduced, but responses near twice the fundamental and at very low frequencies are eliminated entirely. This would indeed be a desirable property for the out-of-plane flapping dynamics of the rotor.

6.3 Wind Tunnel Model Results

Given the successful demonstration of the control concept on the analog simulation, tests were run on the actual rotor in the wind tunnel. Open-loop excitation runs were performed first to extract the system coefficients on which to base the control design. Initial efforts to estimate these periodic parameters were hampered by the presence of extraneous fluctuations and strong levels of periodicity in the transducer signals. Due to the controlled and benign nature of the analog simulation, no special measures were found necessary to identify the parameters for that situation. For the rotor data, however, two additional features had to be incorporated in the parameter estimation scheme: inclusion of additional "forcing" terms, and a change in sampling speed.

The need for additional terms in the identified model can be best understood by considering the effect of a bias present in any of the pitch, flap, flap rate or flap acceleration signals of equation (4.5.1). These biases would get multiplied by the periodic coefficients and show up as spurious harmonics present in the flapping acceleration estimate. By combining the effects of all these biases, one can account for their contribution to the estimation error quite easily. If (4.5.3) is extended to include the terms:

$$\ldots + 1 + \cos(\ ) + \sin(\ ) + \cos(2\ ) + \sin(2\ ) + \cos(3\ )$$

$$+ \ldots] * [\ f0\ f1c\ f1s\ f2c\ f2s\ f3c\ \ldots\ ]$$

then these free coefficients can be solved for at the same time as the periodic parameters using the same technique. Incorporation of these additional terms into the math model also accounts for responses due to any higher harmonic rotor wake effects.

Even though the non-dimensional first out-of-plane bending frequency was at seven times rotor rotation speed, the tip accelerometer was corrupted by a significant amount of vibration energy. This tended to force the initial parameter estimates to have a larger higher harmonic content than was predicted by the quasi-steady theory. In order to eliminate this effect, the FM tape recorder was played back at a higher speed through the anti-aliasing filters, and the data was sampled at 32 samples per revolution, half its normal rate. This effectively doubled the number of rotor cycles present in any given data file, and significantly improved the quality of the identified parameters. It should be pointed out that the time constants of the observer had to be appropriately reduced in order to allow it to track the higher frequencies present.

Results of the parameter estimation routine are plotted in figures 18a, 18b and 18c for open- and closed-loop cases at an advance ratio of 1.4. Even for this severe case of reverse flow over the rotor, the periodicity of the system can be seen to be reduced. All the coefficients exhibit tendencies to approach a constant value with the addition of closed-loop control. The level of reduction is not as dramatic as for the analog simulation due to the model blade's low Lock number (requiring a higher gain value) and the particular choice of model-following cost. However, these results show that periodic control of rotor blade dynamics in the rotating frame is definitely possible even for rather extreme flight conditions.

7. Conclusions

The modal control of individual helicopter rotor blades in the rotating frame has been shown to be possible through demonstration of a digital control system on a model rotor in a wind tunnel. This was achieved through an extension of model-following modern control methods to handle periodic systems. Incorporation of a novel observer structure using acceleration measurements permitted reconstruction of missing state variables, as well as provided sufficient information to identify the periodic parameters of the system.

References

1. Ham, N. D. and McKillip, R. M., Jr., "A Simple System for Helicopter Individual-Blade-Control and Its Application to Gust Alleviation", Proc. Thirty-Sixth AHS National Forum, May 1980.

2. Zwicke, P. E., "Helicopter Gust Alleviation: An Optimal Sampled-Data Approach", Proc. Thirty-Sixth AHS National Forum, May 1980.

3. Ham, N. D. and Quackenbush, T. R., "A Simple System for Helicopter Individual-Blade-Control and Its Application to Stall-Induced Vibration Alleviation", Proc. AHS National Specialists Meeting on Helicopter Vibration, Hartford, Connecticut, November 1981.

4. Shaw, J. and Albion, N., "Active Control of Rotor Blade Pitch for Vibration Reduction: A Wind Tunnel Demonstration", Vertica, V.4, n.1, 1980.

5. Wood, E. R., "Higher Harmonic Control for the Jet Smooth Ride", Vertiflite, V.29, n.4, 1983, pp. 28-32.

6. Rahnema, M. "Alleviation of Helicopter Fuselage-Induced Rotor Unsteady Loads Through Deterministic Variation of the Individual Blade Pitch", NASA CR-166234, 1981.

7. Ham, N. D., Behal, B. L. and McKillip, R. M., Jr., "Helicopter Lag Damping Augmentation Through Individual-Blade-Control", Vertica, V.7, n.4, 1983.

8. Molusis, J. A., Hammond, C. E. and Cline, J. H., "A Unified Approach to the Optimal Design of Adaptive and Gain Scheduled Controllers to Achieve Minimum Helicopter Rotor Vibration", Proc. Thirty-Seventh AHS Annual National Forum, May 1981.

9. Johnson, W., "Self-Tuning Regulators for Multicyclic Control of Helicopter Vibration", NASA TP-1996, March 1982.

10. Taylor, R. B., Zwicke, P. E., Gold., P. and Miao, W., "Analytical Design and Evaluation of an Active Control System for Helicopter Vibration and Gust Response Alleviation", NASA CR-152377, July 1980.

11. Kretz, M., "Research in Multicyclic and Active Control of Rotary Wings", Vertica, V.1, n.2, 1976.

12. Ham, N. D., "A Simple System for Helicopter Individual-Blade-Control Using Modal Decompisition", Vertica, V.4, n.1, 1980.

13. Guinn, K. F., "Individual Blade Control Independent of a Swash Plate", Journal of the AHS, V.27, n.3, July 1982.

14. Ham, N. D., "Helicopter Individual-Blade-Control and Its Applications", Proc. Ninth European Rotorcraft Forum, Stresa, Italy, September 1983.

15. Johnson, W. Helicopter Theory. Princeton University Press, Princeton, New Jersey, 1980.

16. McKillip, R. M., Jr., "Periodic Control of the Individual Blade Control Helicopter Rotor" , M.I.T. VTOL Technology Laboratory TR 196-7, August 1984.

17. Tyler, J., Jr., "The Characteristics of Model-Following Systems as Synthesized by Optimal Control", IEEE Trans. on Automatic Control, V.AC-9, n.4, 1964, pp.485-498.

18. Kreindler, E. and Rothschild, D., "Model-Following in Linear-Quadratic Optimization", AIAA Journal, V.14, n.7, July 1976, pp. 835-842.

19. Kriechbaum, G. and Stineman, R., "Design of Desirable Airplane Handling Qualities via Optimal Control", AIAA Journal of Aircraft, V.9, n.5, 1972, pp.365-369.

20. Bryson, A. E., Jr. and Ho, Y. Applied Optimal Control. John Wiley and Sons, New York, 1975.

21. Kwakernaak, H. and Sivan, R. Linear Optimal Control Systems. Wiley-Interscience, New York, 1972.

22. Nishimura, T., "Spectral Factorization in Periodically Time-Varying Systems and Application to Navigation Systems", AIAA J. of Spacecraft and Rockets, V.9, n.7, 1972, pp. 540-546.

23. Dugundji, J. and Wendell, J. H., "Some Analysis Methods for Rotating Systems with Periodic Coefficients", AIAA Journal, V. 21, n.6, 1983, pp.890-897.

24. Friedmann, P., Hammond, C. E. and Woo, T., "Efficient Numerical Treatment of Periodic Systems with Application to Stability Problems", Int. J. for Numerical Methods in Engineering, V.11, 1977, pp. 1117-1136.

25. D'Angelo, H. Linear Time-Varying Systems: Analysis and Synthesis. Allyn and Bacon, Boston, 1970.

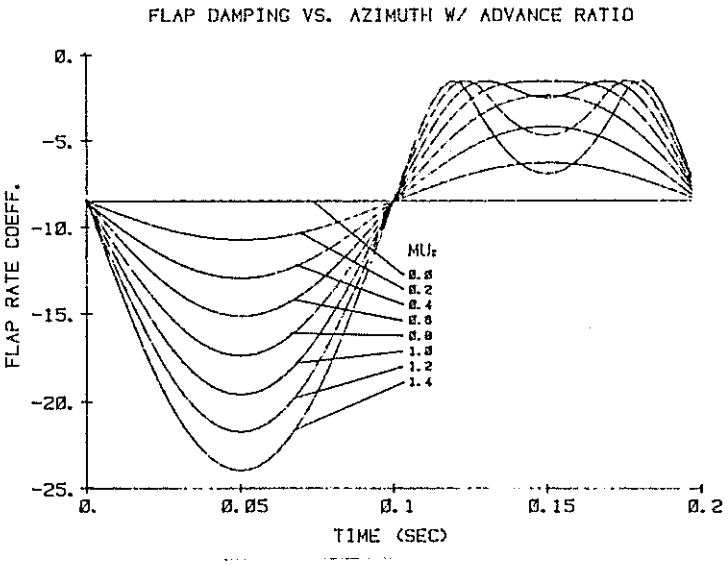

Fig. 1: Flap damping (inverted) versus time for Ω = 5 Hz

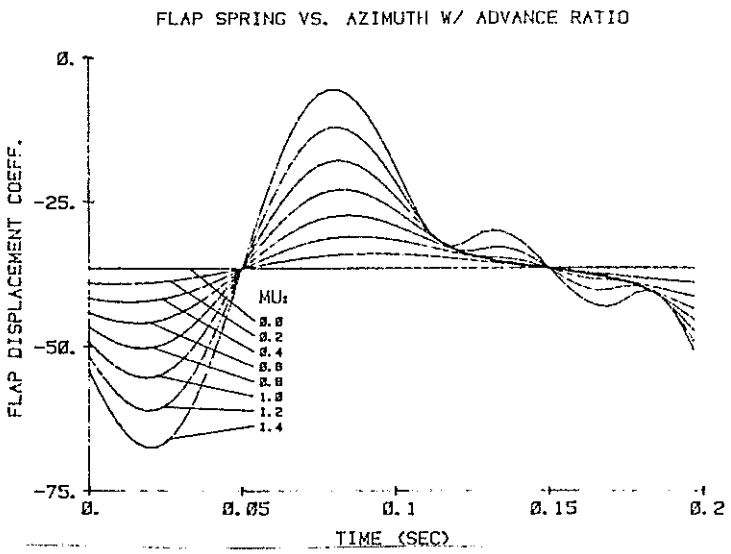

Fig. 2: Flap spring (inverted) versus time for Ω = 5 Hz

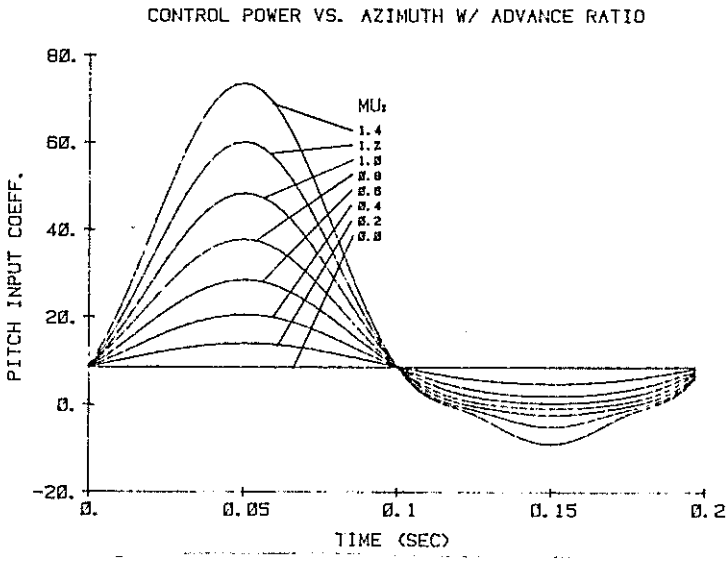

Fig. 3: Pitch control power versus time for Ω = 5 Hz

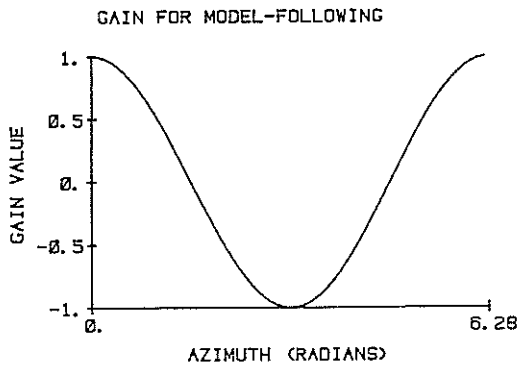

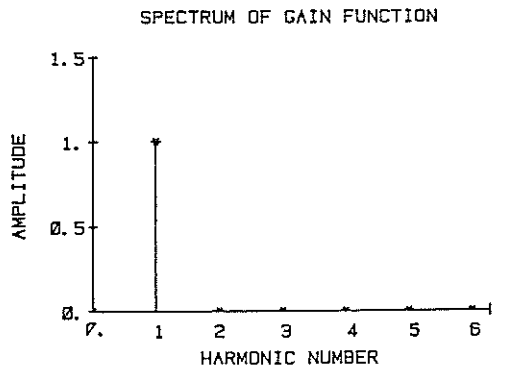

Fig. 4: Feedback gain for scalar example

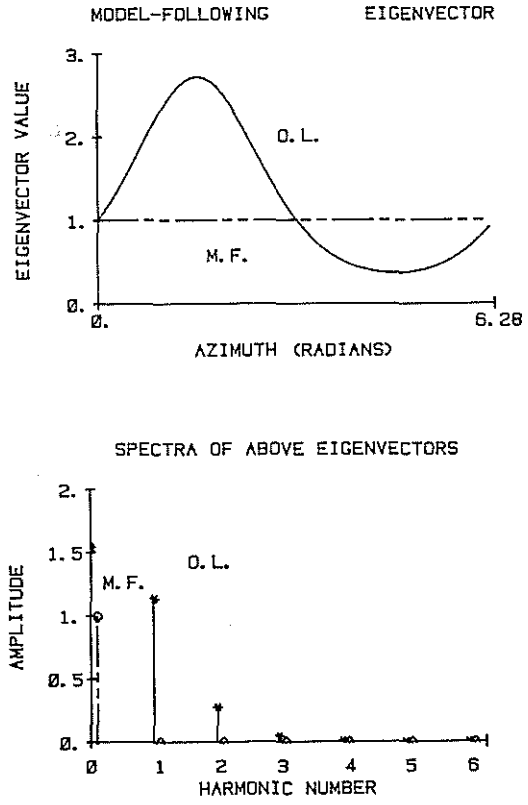

Fig. 5: Open- and closed-loop eigenvector for scalar model-following example

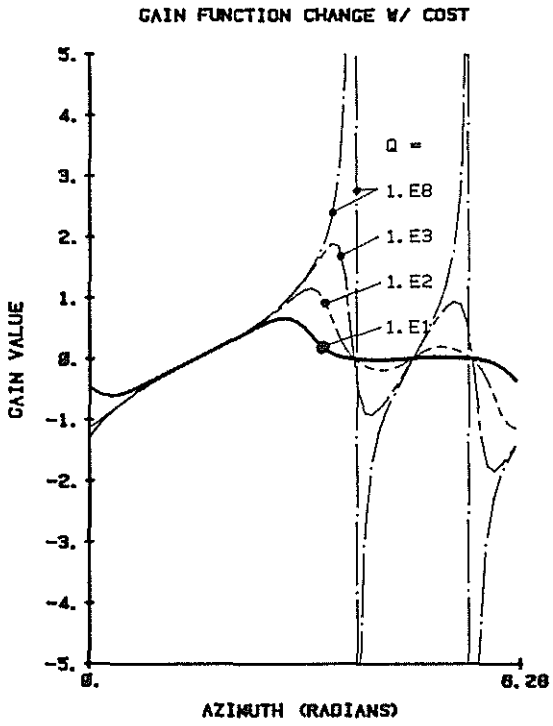

Fig. 6: Gain function for various cost values at μ=1.4

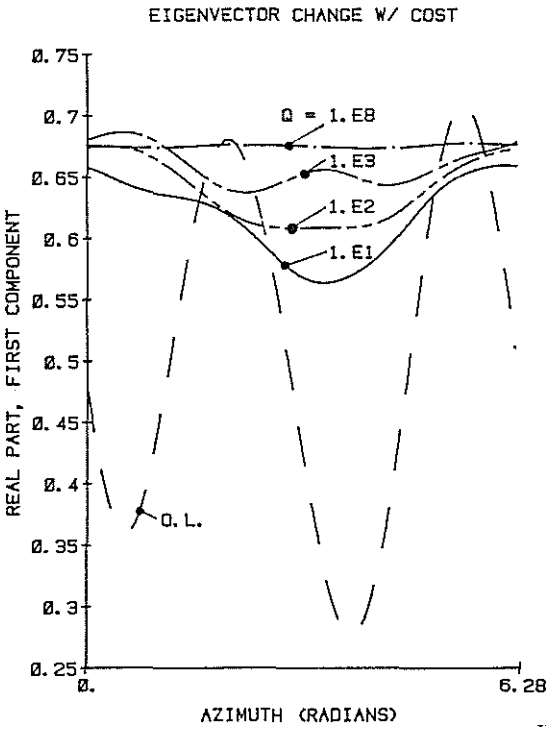

Fig. 7: Eigenvector component for μ=1.4 with increasing levels of model-following cost

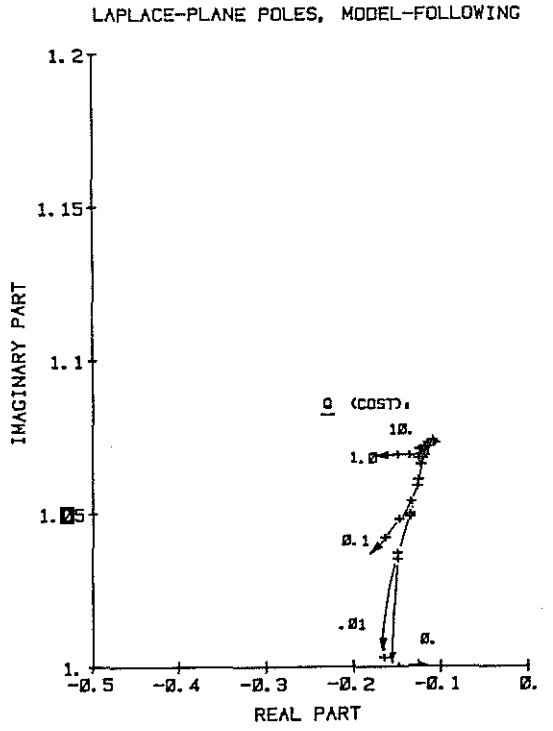

Fig. 8a: Laplace-plane root loci for increasing advance ratio at a fixed model-following cost

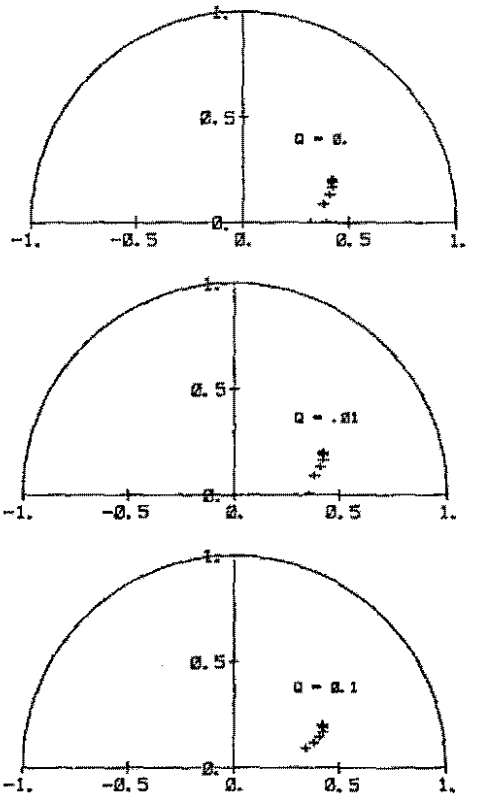

Fig. 8b: Floquet-plane root loci for increasing advance ratio at a fixed model-following cost

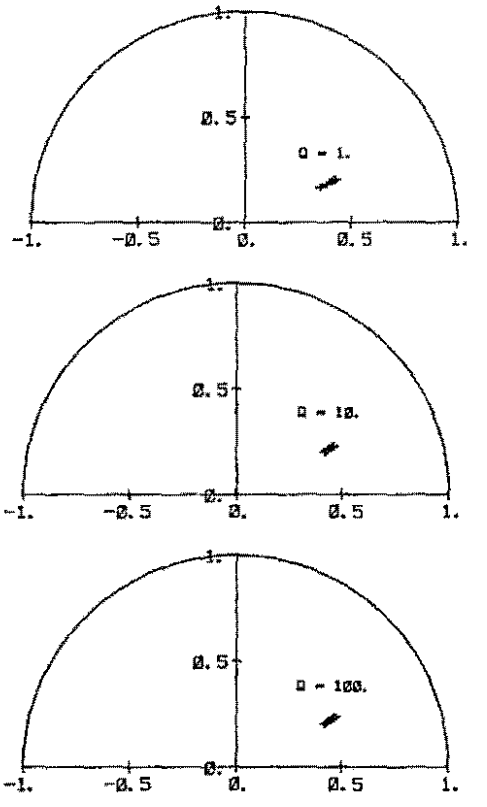

Fig. 8c: Floquet-plane root loci for increasing advance ratio at a fixed model-following cost

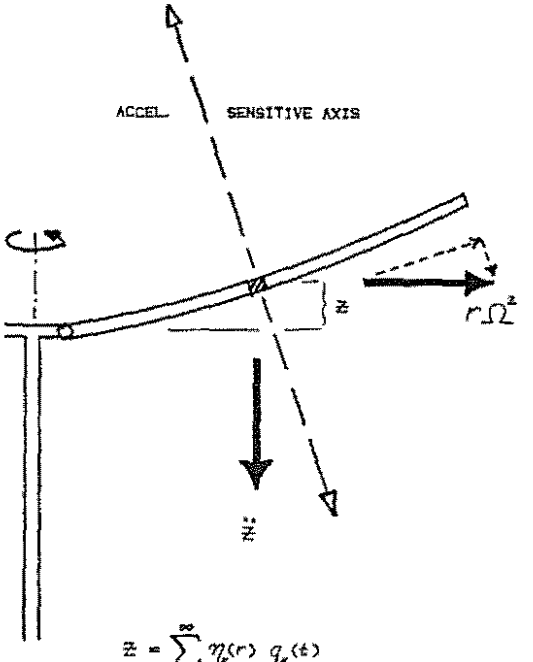

$$\ddot{z} = \sum_{K=1}^{\infty} \eta_K(r)\, \ddot{q}_K(t)$$

$$\text{ACCEL} = \sum_{K=1}^{\infty} \left\{ \eta_K \ddot{q}_K + r\Omega^2 \frac{d}{dr}\eta_K q_K \right\}$$

Fig. 9: Sensor dynamics for tip accelerometer

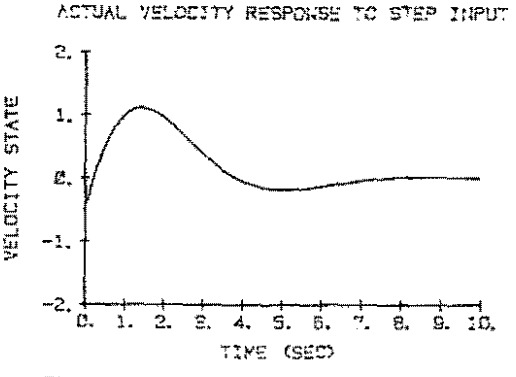

Fig. 10a: Velocity state of digital simulation

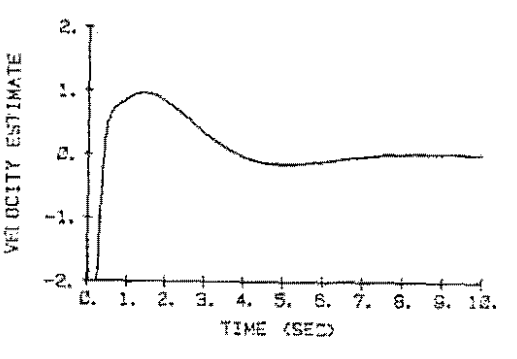

Fig. 10b: Estimated velocity using second-order Kalman Filter

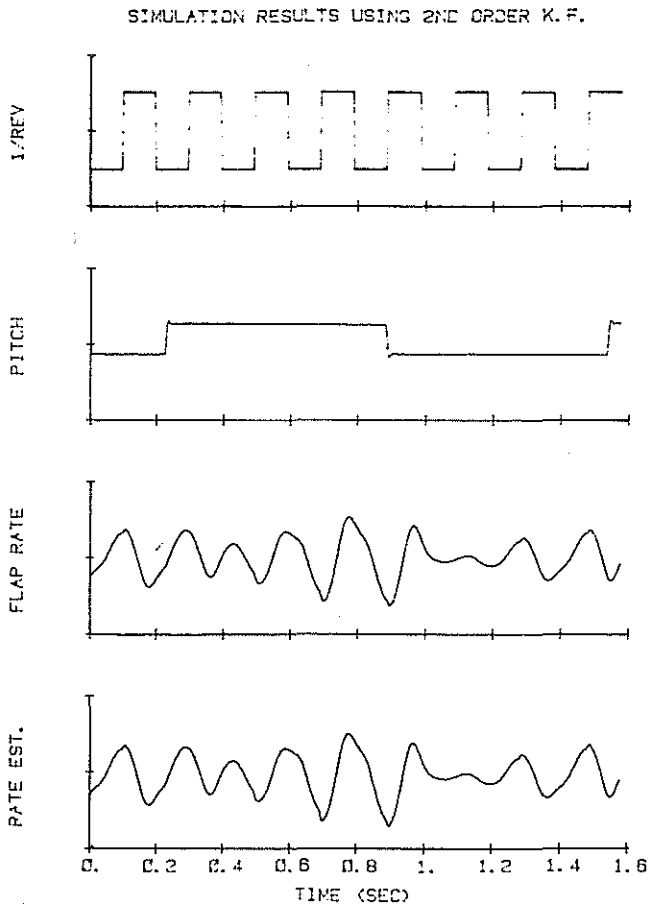

Fig. 11: Comparison of actual and estimated flapping rate estimate for analog simulation, μ=1.14

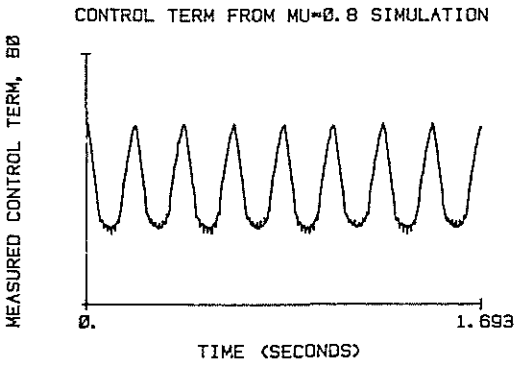

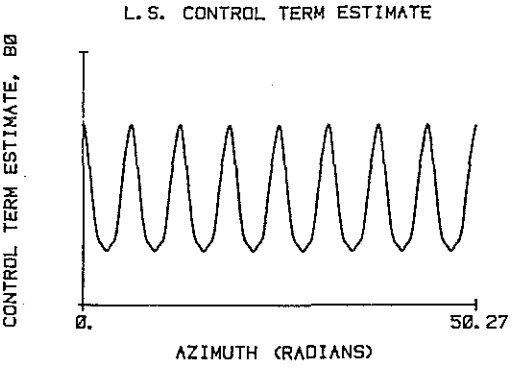

Fig. 12a: Comparison of actual and estimated periodic control term from parameter regression

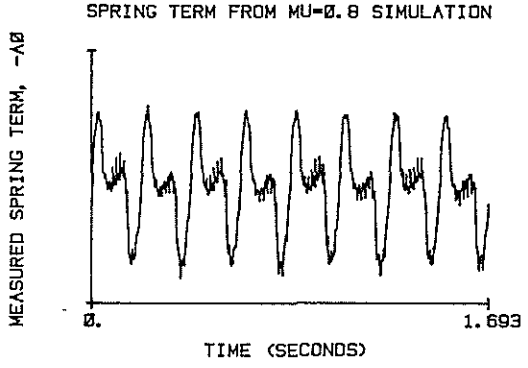

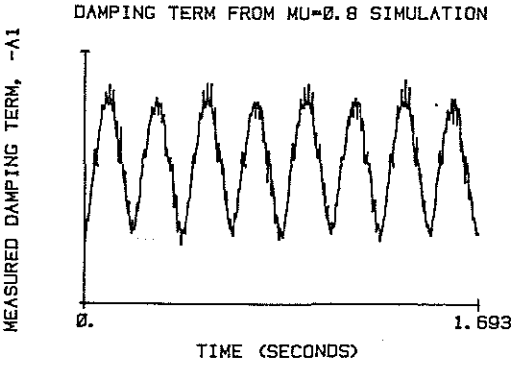

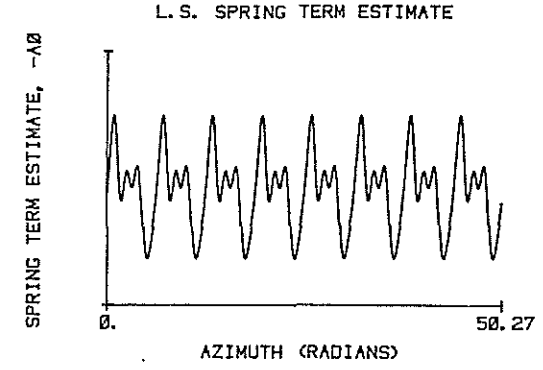

Fig. 12b: Comparison of actual and estimated periodic spring term from parameter regression

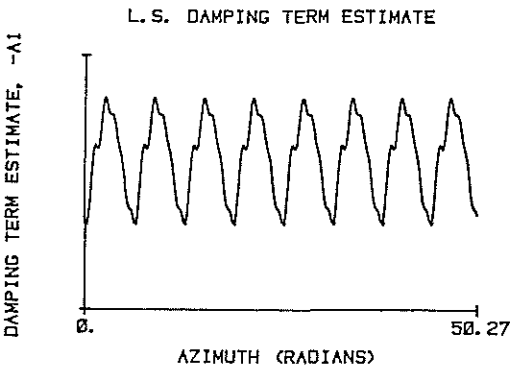

Fig. 12c: Comparison of actual and estimated periodic damping term from parameter regression

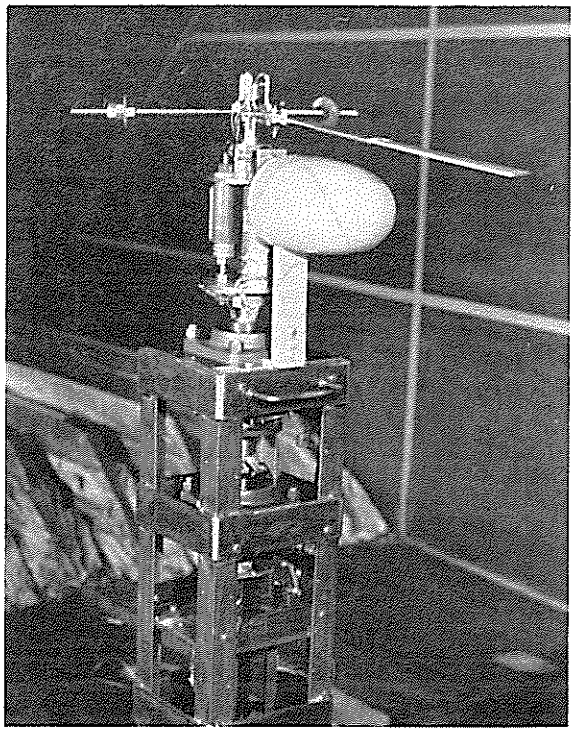

Fig. 13: IBC model rotor installed in acoustic tunnel

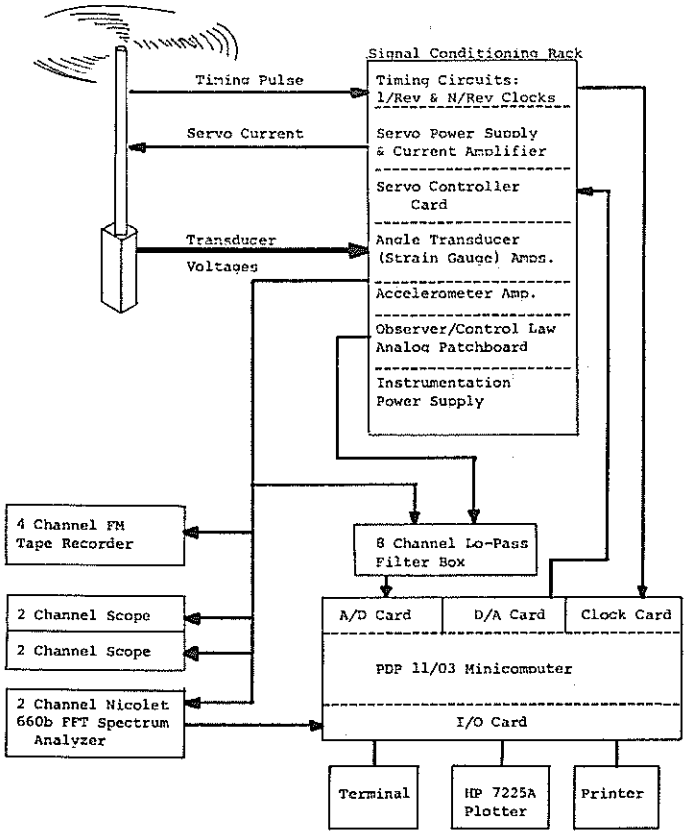

Fig. 14: Instrumentation schematic for data collection

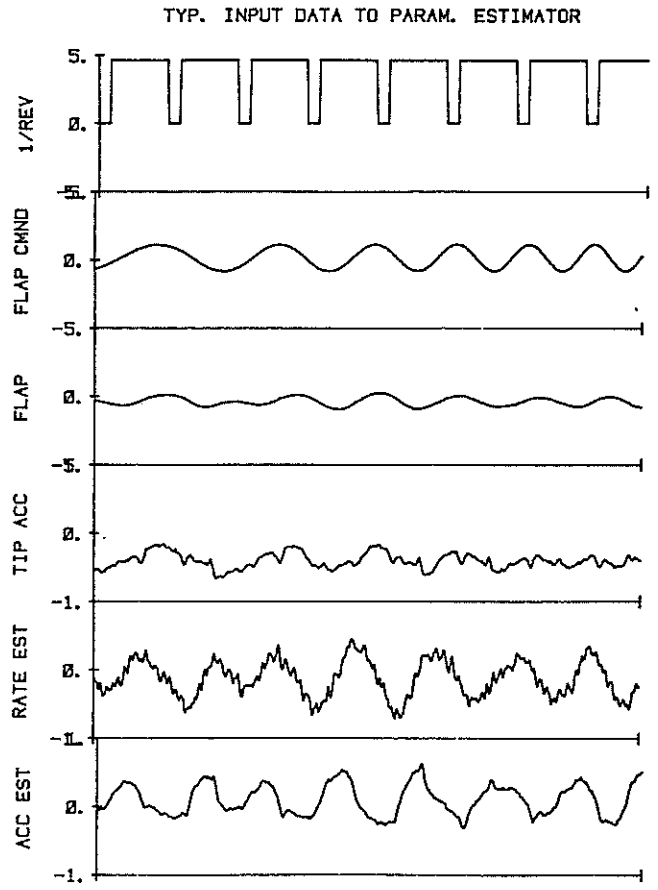

Fig. 15: Typical data set for parameter identification

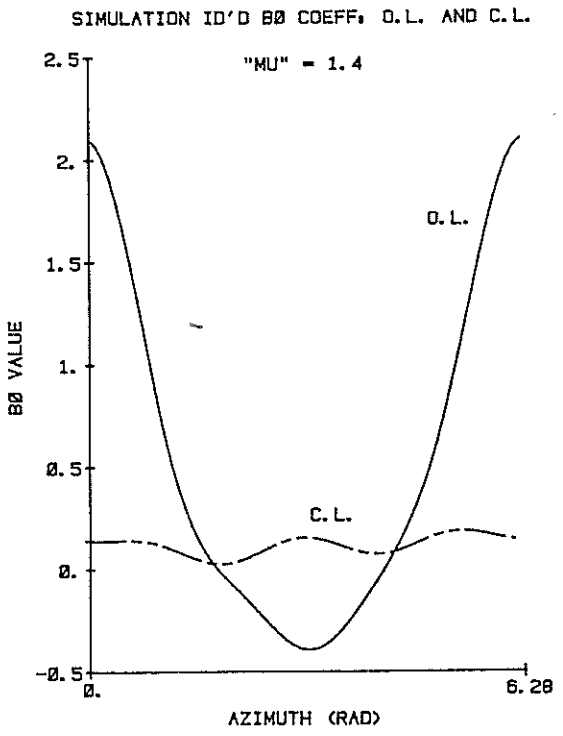

Fig. 16a: Estimated control power for simulation, open- and closed-loop

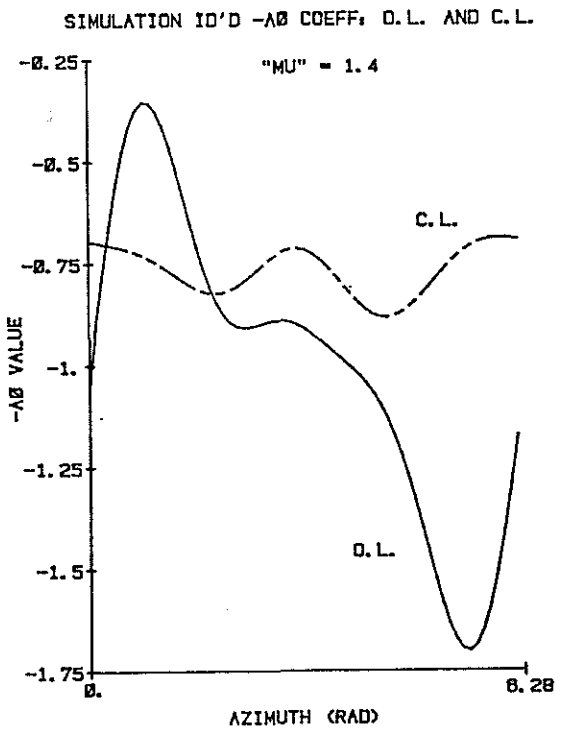

Fig. 16b: Estimated spring term for simulation, open- and closed-loop

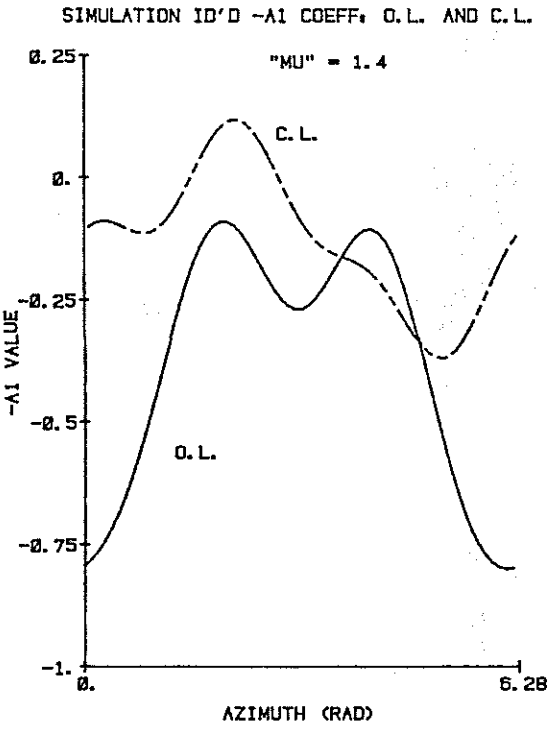

Fig. 16c: Estimated damping term for simulation, open- and closed-loop

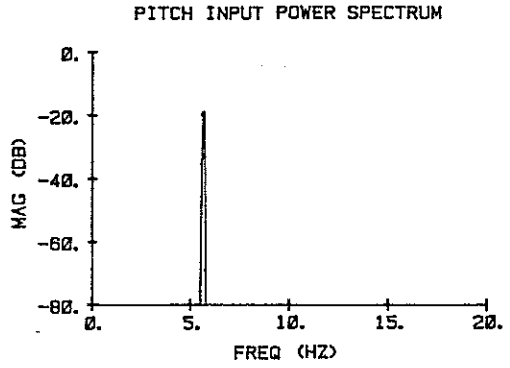

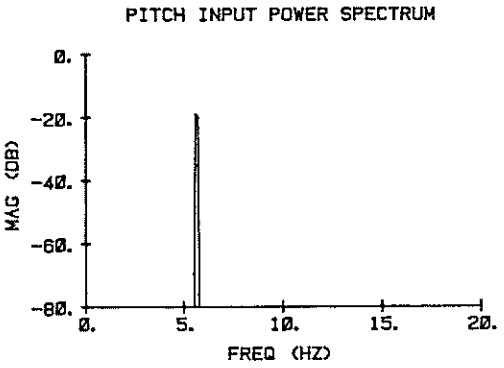

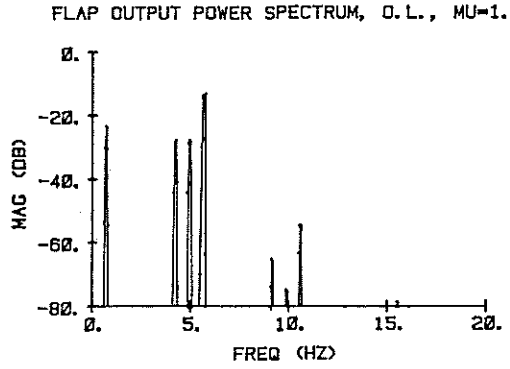

Fig. 17a: Open-loop power sprectra for simulation of excitation and response

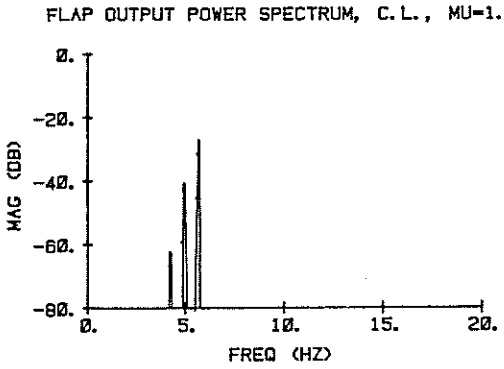

Fig. 17b: Closed-loop power spectra for simulation of excitation and response

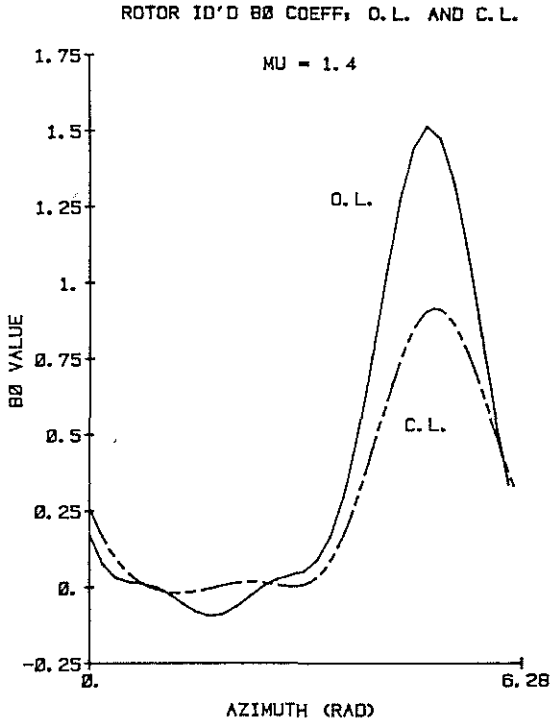

Fig. 18a: Estimated control power for rotor, open- and closed-loop

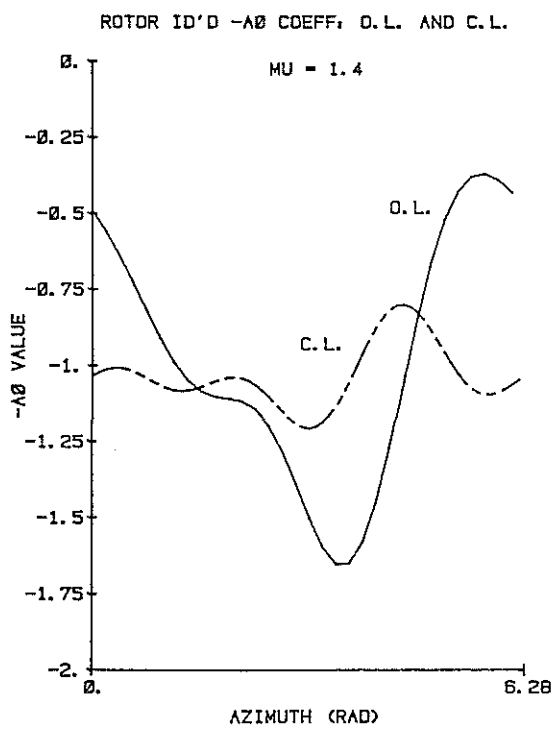

Fig. 18b: Estimated spring term for rotor, open- and closed-loop

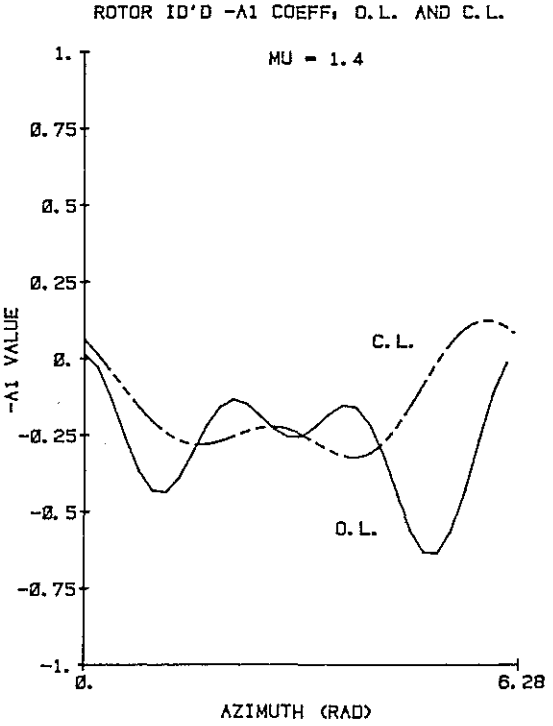

Fig. 18c: Estimated damping term for rotor, open- and closed-loop